Supplementary Information (SI) for Energy & Environmental Science.
This journal is © The Royal Society of Chemistry 2026

Supplementary Information

Stabilizing the Buried Interface *via* Inorganic-Organic Hybrid Layers for High-Performance Perovskite Photovoltaics

Yulin Xie[1], Ziwei Zheng[2], Huazhong Liu[1], Lin Li[3]*, Kai Gao[3]*, Xiong Li[2]*

[1]School of Physics and Electronic Information, Huanggang Normal University, Huanggang 438000, Hubei Province, China.

[2]School of Physics and Optoelectronic Engineering, Hainan University, Haikou 570228, China.

[3]Institute of New Materials and Advanced Manufacturing, Beijing Academy of Science and Technology, Beijing, 100089, China.

Corresponding author:

Lin Li, e-mail address: lilin1@bjast.ac.cn

Kai Gao, e-mail address: Gaokai@bjast.ac.cn

Xiong Li, e-mail address: li-xiong@hainanu.edu.cn

Experimental Section

Materials

Raw material, including lead iodide (PbI_2, 99.999%), cesium iodide (CsI, >99.999%), and formamidinium iodide (FAI, >99.5%), was purchased from Xi'an Yuri Solar Co., Ltd. The silicon dioxide (SiO_2, 20 wt% dispersity in ethanol) with a particle size of 30 nm is sourced from Shanghai Macklin Biochemical Technology Co., Ltd. The (4-(7H-dibenzo[c,g]carbazol-7-yl)butyl)phosphonic acid (4PADCB, >99.0%) was sourced from Shanghai Weizhu Chemical Technology Co., Ltd. C60 and bathocuproine (BCP) were purchased from Xi'an Polymer Light Technology Corporation (China). All chemicals and reagents were used as received from chemical companies without any further purification. The solvents, including dimethylformamide (DMF, 99.8%), dimethyl sulfoxide (DMSO, 99.7%), isopropanol (IPA), and chlorobenzene (CB, 99.8%) were purchased from Thermo Fisher Scientific and used without further purification. High-purity silver was purchased from commercial sources. The glass substrates patterned with indium tin oxide (ITO) were received from Shangyang Technology Co., Ltd.

Perovskite solar cells (PSCs) fabrication

Glass/ITO substrates were sequentially cleaned by ultrasonication in detergent, deionized water (twice), and ethyl alcohol for 15 min each. Then, the glass/ITO substrates were dried with nitrogen and subsequently treated with oxygen plasma for 20 minutes. They were then transferred into an N_2-filled glovebox before use. In this work, (4-(7H-dibenzo[c,g]carbazol-7-yl)butyl)phosphonic acid (4PADCB) was used as the hole transport layers (HTLs). Three types of HTLs were prepared. For the pristine 4PADCB HTL, 4PADCB powder was dissolved in anhydrous ethanol at a concentration of 0.5 mg mL^{-1}, spin-coated onto ITO substrates at 3,000 rpm for 30 s, and then annealed at 100 °C for 10 min in a N_2-filled glovebox. For the SiO_2-modified composite HTL, a 20 wt% SiO_2 commercial stock dispersion in ethanol was first diluted to 0.4 wt%. The diluted SiO_2 dispersion was then mixed with the 4PADCB solution (0.5 mg mL^{-1}) to achieve a final SiO_2-to-4PADCB mass ratio of 28 wt% in the mixed solution. The mixture was stirred for 15 min, then spin-coated onto ITO substrates at 3,000 rpm for 30 s, followed by annealing at 100 °C for 10 min in a N_2-filled glovebox. For the pre-mixed HTL prepared by a two-step spin-coating procedure, the 4PADCB film was first deposited onto the ITO substrate following the same procedure as the pristine 4PADCB HTL. Subsequently, the SiO_2 dispersion (at the same concentration used for the mixed solution) is spin-coated onto the pre-formed 4PADCB layer at 3,000

rpm for 30 s, followed by annealing at 100 °C for 10 min in a N_2-filled glovebox to obtain the ITO / 4PADCB / SiO_2 configuration.

For perovskite precursor preparation, a 1.5 M perovskite precursor solution was prepared by mixing 19.5 mg of CsI, 245.06 mg of FAI, 10.13 mg MACl and 712.24 mg of PbI_2 (10% of excess) in 1 mL DMF: DMSO (4:1 in volume) mixed solvent with a chemical formula of $Cs_{0.05}FA_{0.95}PbI_3$ to form a 1.53 eV perovskite. All steps were conducted in an N_2-filled glove box. For 1.53 eV perovskite films fabrication, the perovskite precursor was spin-coated on the as-prepared substrates with HTLs at 2,000 rpm for 10 s, subsequently at 4,000 rpm for 40 s, during which 150 μL CB was dripped onto the center of the film at 5 s before the end of spin-coating. The substrates were immediately transferred to the hot plate and annealed at 100 °C for 30 minutes. For devices with surface passivation treatment, PEAI was dissolved in IPA (1 mg mL^{-1}) and spun onto the as-prepared perovskite films at 5,000 rpm. for 30 s, followed by annealing at 100 °C for 5 min. The spin-coating processes were conducted in an N_2-filled glovebox with a controlled temperature of 20-23 °C, maintained by the integrated air conditioner, and the water and oxygen levels were both controlled at less than 5 ppm. Finally, 20 nm C60 was thermally evaporated at 0.1 Å/s, 7 nm BCP at 0.1 Å/s, and a 100 nm silver electrode at 0.5 Å/s, respectively, under a high vacuum ($< 4 \times 10^{-5}$ Torr). The device area was defined and characterized as 0.0815 cm^2 by a metal shadow mask.

Characterizations

The particle size distribution of the SAMs, both without and with different inert oxide precursor solutions in ethanol, was measured using a dynamic light scattering particle size analyzer (DLS, Malvern Zetasizer Nano ZS90) at 25 °C with a monochromatic coherent He-Ne laser (λ = 632.8 nm) as the light source. An avalanche photodiode detector that detected scattered light at 90°. The perovskite precursor contact angles on HTLs-coated substrates were measured using an SDC-200Z automated contact angle goniometer (SINDIN, China) at 25°. An automatic syringe dispensed a droplet (2 μL), and images were analyzed by the Young-Laplace fitting method. The X-ray Photoelectron Spectroscopy (XPS) measurements were performed on a Kratos AXIS-ULTRA DLD-600W system with a monochromatic Al Kα source (1486.6 eV). All spectra were calibrated using the C 1s peak of adventitious carbon (284.8 eV) as an internal reference. Contact potential difference (CPD) was performed using an Oxford Instruments Asylum Research AFM equipped with a Kelvin Probe Force Microscopy (KPFM) module.

Measurements were conducted in tapping mode using a Pt/Ir-coated conductive tip (ASYELEC-01, spring constant ~2 N/m), under ambient conditions (25°C, 40% relative humidity). X-ray diffraction (XRD) data were collected in reflection mode at room temperature using the Rigaku MiniFlex, equipped with monochromated Cu Kα (λ = 1.54 Å, 15 mA, 40 kV) radiation. Ultraviolet-visible (UV-vis) absorption spectra were measured using a UV-vis spectrometer (Shimadzu UV-2600). The surface and cross-section scanning electron microscope (SEM) morphology of the HTLs and perovskite films was acquired by field-emission scanning electron microscopy (FEI Nova NanoSEM 450). Steady-state photoluminescence (PL) spectra were measured using a Horiba Fluorolog-QM modular spectrofluorometer with an excitation source at 532 nm wavelength. A Horiba DeltaFlex-01 fluorimeter was used to measure the time-resolved photoluminescence (TRPL) spectra. The external quantum efficiency (EQE) was measured in DC mode (zero-bias condition unless specified) using the Saifan EQE system, a monochromatic technology employed in this paper. The fluorescence lifetime imaging microscopy (FLIM) spectra were measured using FLIM 300. Transient photovoltage (TPV) and transient photocurrent (TPC) measurements, and Mott-Schottky plots were obtained using a Zennium electrochemistry workstation (Zahner, Germany). The current-voltage (J-V) curves were measured using a solar simulator (Oriel 94023A, 300 W) with a source meter (Keithley 2400) under 100 mW cm^{-2} illumination (AM 1.5G) at a scan rate of 10 mV s^{-1}. The operational stability tests were conducted at the MPP for the unencapsulated cells under one sun illumination (100 mW cm^{-2}) at 65 °C with 50% ± 5% humidity.

Supplementary Note 1: Analysis of Supplementary Figure 11

For Depth-profiling XRD measurement, the (210) plane of perovskite featuring an XRD peak at 31.6° was selected was chosen as the stress-free 2θ degree due to its diversity in providing more reliable structure symmetry information, in which the 2θ is fixed while the instrument tilt angles were varied to ensure the X-ray penetration depth. The tilt angles (ψ) were fixed at 5°, 15°, 25°, 35°, and 45°, respectively. According to Bragg's Law and generalized Hooke's Law, the relationship of 2θ-$\sin^2\psi$ can be given by the following equation[1]：

$$\sigma = \frac{E_p}{1+\nu_p}\frac{\pi}{180^{\circ}}\cot\theta_0\frac{\partial(2\theta)}{\partial\sin^2\psi} \tag{S1}$$

where E_p is the perovskite modulus (10 GPa) and ν_p is Poisson's ratio of the perovskite 0.3.[2] θ_0 is

half of the scattering angle $2\theta_0$ for stress-free perovskite ($2\theta_0$ = 31.6°). The residue stress of perovskite films can be calculated from equation (S1) by fitting the 2θ as a function of $\sin^2\psi$, and the slope of the fitted line represents the scale of the residual strain. The negative slope indicates the films bear tensile stress, while the positive slope indicates the films bear compressive stress.

Supplementary Note 2: Analysis of Supplementary Figure 16

A double exponential function equation fitted the TRPL spectra：

$$I(t)=I_0+A_1\exp(-t/\tau_1)+A_2\exp(-t/\tau_2) \quad \text{(S2)}$$

where A_1 and A_2 represent the decay amplitude of the fast and slow decay processes, respectively. τ_1 and τ_2 represent the fast and slow decay time constants, respectively. The average carrier lifetime (τ_{ave}) was calculated by using the equation of $\tau_{ave}=(A_1\tau_1^2+A_2\tau_2^2)/(A_1\tau_1+A_2\tau_2)$.

Supplementary Note 3: Analysis of space charge-limited current (SCLC)

The conductivity σ can be determined from the space charge-limited current (SCLC) model using hole-only devices with the configuration ITO/ 4PADCB or SiO_2-modified HTLs/Ag, according to the equation below:[3]

$$\sigma = \frac{k}{A}d \quad \text{(S3)}$$

Where k is the slope of the hole-only carrier devices J-V curve, A is the area, and d is the thickness of HTL. Note that because SiO_2 nanoparticles are electrically insulating, they act as an inactive scaffold. The hole transport exclusively percolates through the 4PADCB molecular pathways. Thus, the effective charge-transport thickness (d) of both films is defined by the organic molecular layer (~10 nm).[4]

And the hole mobility (μ) is calculated by the Mott-Gurney law:

$$\mu = \frac{8d^3}{9\varepsilon_r\varepsilon_0}\left(\frac{\sqrt{J}}{V}\right)^2 \quad \text{(S4)}$$

Where the ε_0 and ε_r are the vacuum dielectric constant and relative dielectric constant of the HTL material, respectively, with $\varepsilon_r = 2.5$.[5] V is the applied voltage, and J is the current density.

Supplementary Note 4: Calculation of the quasi-Fermi level splitting (QFLS) based on the PL quantum yield (PLQY)

To investigate the non-radiative recombination at the interface between different hole-selective layers and perovskite, we calculated the Quasi-Fermi level splitting (QFLS) values of 1.53 eV bandgap perovskite films on a bare glass substrate and different HTLs on the ITO substrate by using photoluminescence quantum yield (PLQY) measurements. The QFLS and PLQY as the following equation:[6]

$$\mathrm{QFLS} = \mathrm{QFLS_{rad}} + k_B T \cdot \ln(\mathrm{PLQY}) = k_B T \cdot \ln(\mathrm{PLQY} \cdot J_G / J_{0,rad}) \quad \text{(S5)}$$

Here, QFLS is the difference between the electron and hole quasi-Fermi levels in the perovskite layer, k_B is the Boltzmann constant, and T is the temperature (300 K). J_G is the generation current density under illumination, in this case, approximated to the short-circuit current density J_{SC} of devices. $J_{0,rad}$ is the dark radiative recombination saturation current density.

According to the detailed balance at open-circuit conditions, the $J_{0,rad}$ can be calculated by the following equations:

$$J_{0,rad} = e\int_0^{\infty} EQE_{\mathrm{PV}}(E)\Phi_{BB}(E)dE \quad \text{(S6)}$$

$$\Phi_{BB}(E) = \frac{2\pi E^2}{h^3 c^2} \cdot \frac{1}{\exp(\frac{E}{k_B T}) - 1} \quad \text{(S7)}$$

Where e is the elementary charge, EQE_{PV} is the photovoltaic external quantum efficiency, E is the photon energy, ϕ_{BB} is the black-body radiative spectrum, h is the Planck constant, and c is the light speed in a vacuum. External quantum efficiency (EQE) of the p-i-n PSCs and the emitted spectral photon flux are calculated when the device is in equilibrium with the black-body (BB) radiation (T = 300 K). Based on equations S5 and S6, the $J_{0,rad}$ was calculated similarly as 4.72×10^{-20} A m^{-2} for all systems independent of the bottom charge transport layer.

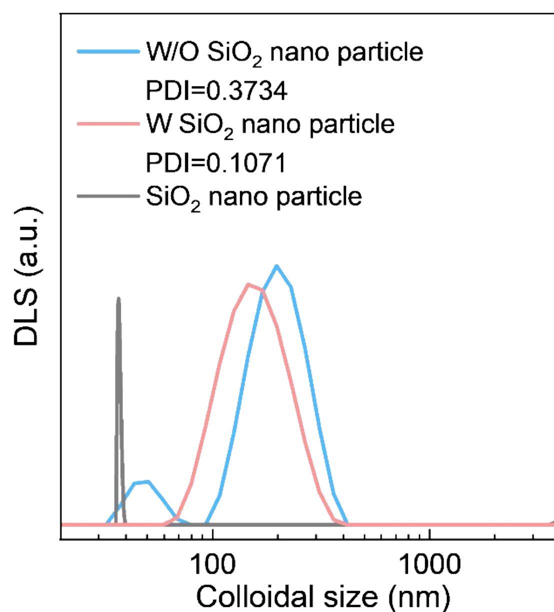

Figure S1. Dynamic light scattering (DLS) analysis of particle size distribution for pristine SAM solution, SAM with SiO_2 nanoparticle solution, and SiO_2 nanoparticle solution.

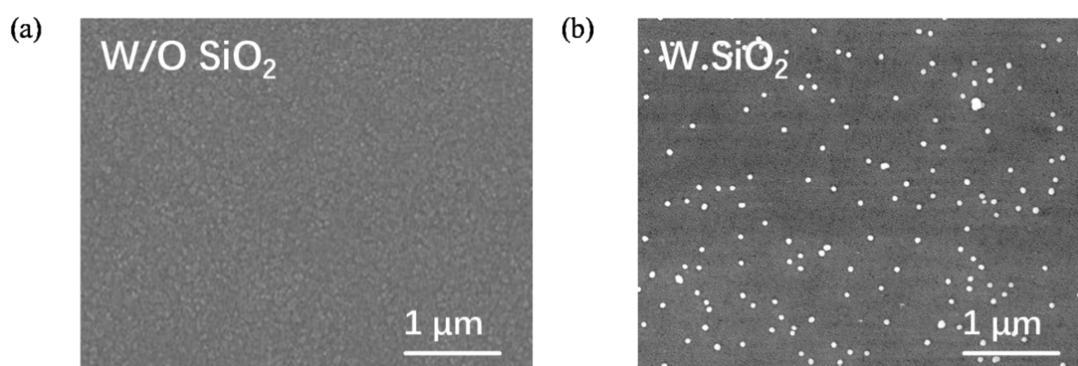

Figure S2. Top-view scanning electron microscope (SEM) of (a) pristine 4PADCB, (b) SiO_2-based HTLs deposited on ITO.

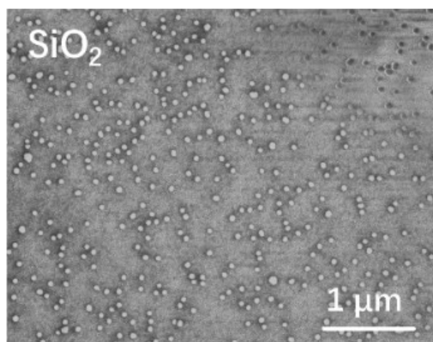

Figure S3. Top-view SEM of pure SiO_2 deposited on ITO.

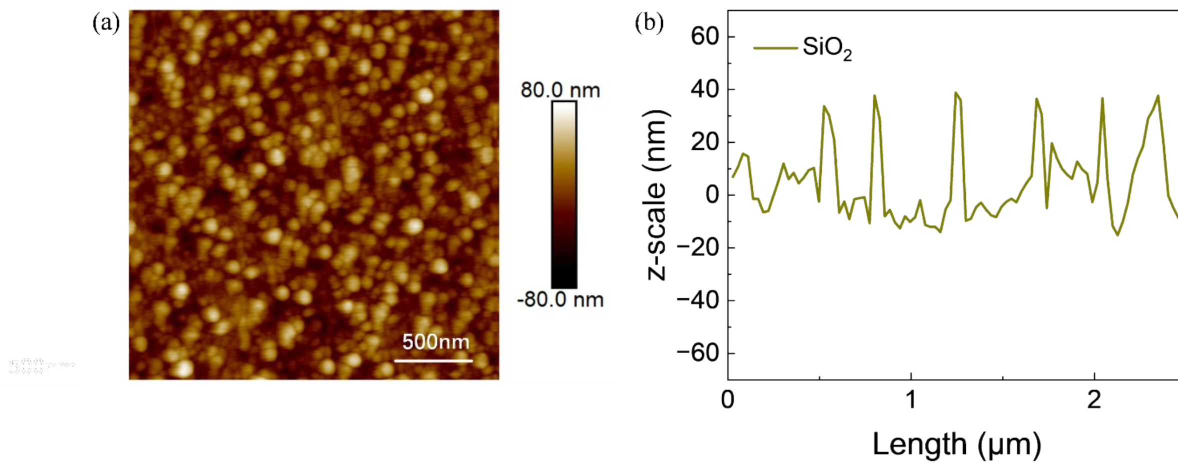

Figure S4. The atomic force microscopy (AFM) height image of pure SiO_2 nanoparticles deposited on ITO and the corresponding representative height profile.

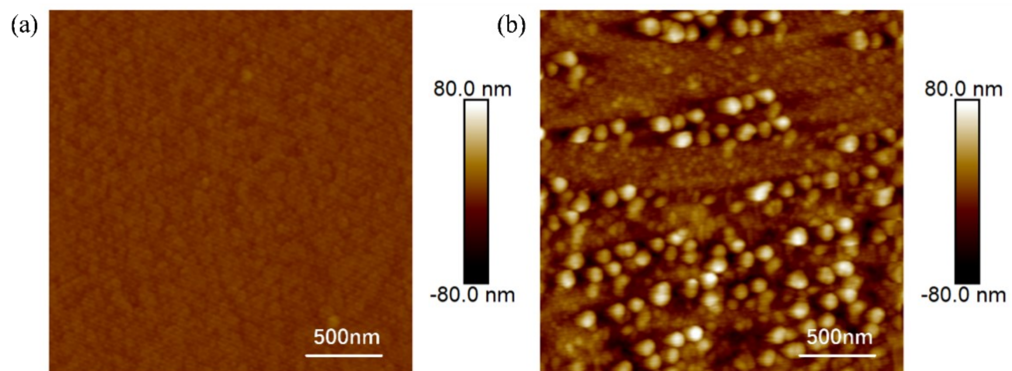

Figure S5. AFM surface morphology of (a) pristine SAM and (b) SiO_2-based hole-selective layer deposited on ITO.

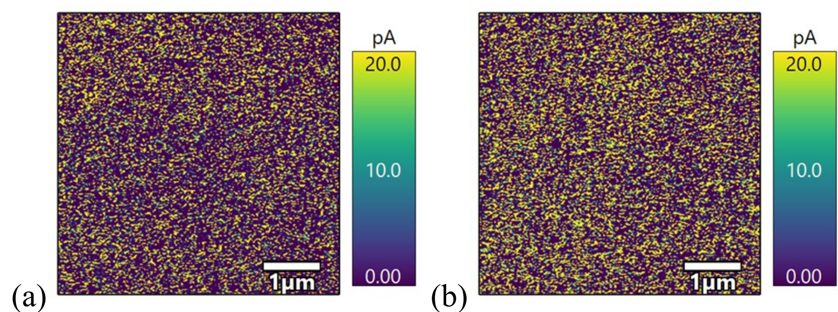

Figure S6. C-AFM current maps of pristine 4PADCB and SiO_2-modified HTL films deposited on ITO, acquired under the same bias and imaging conditions. The comparable nanoscale current response indicates that the discontinuous SiO_2 domains do not form a continuous insulating barrier.

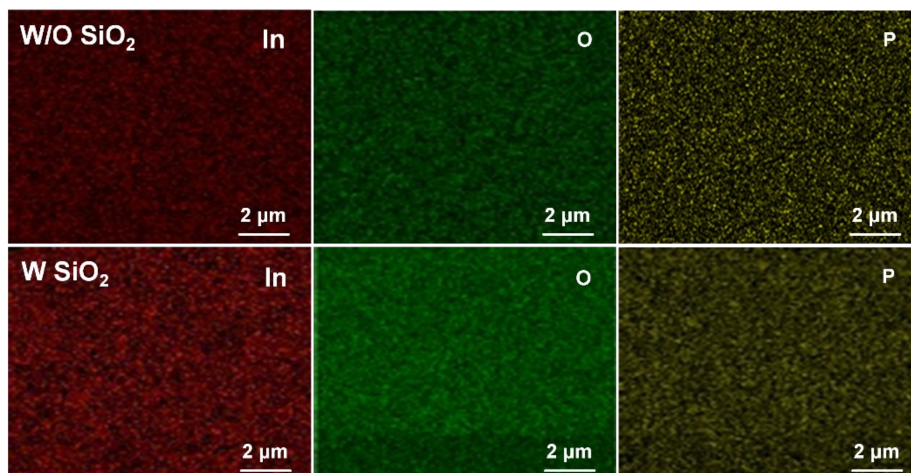

Figure S7. SEM-Energy Dispersive Spectrometer (EDS) of In, O, P elements with pristine 4PADCB and SiO_2-based hole-selective layer deposited on ITO.

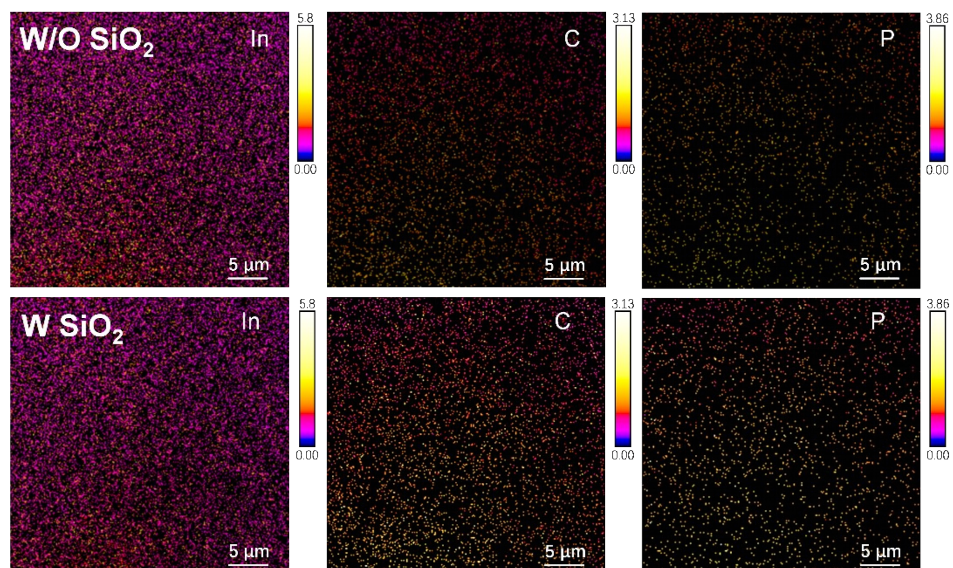

Figure S8. X-ray Photoelectron Spectroscopy (XPS) mapping of pristine 4PADCB and SiO_2-based HTLs deposited on ITO.

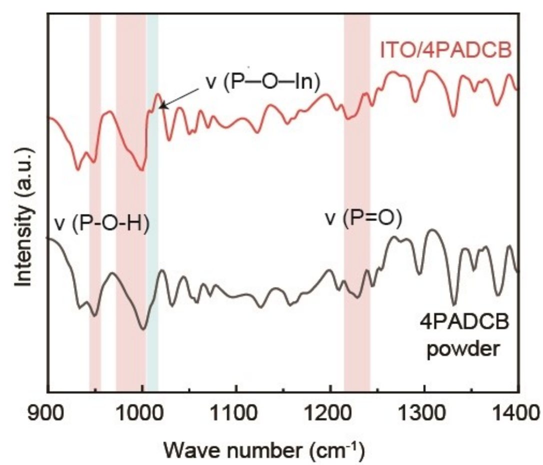

Figure S9. Fourier transform infrared spectroscopy (FTIR) of 4PADCB power and the 4PADCB film deposited on ITO.

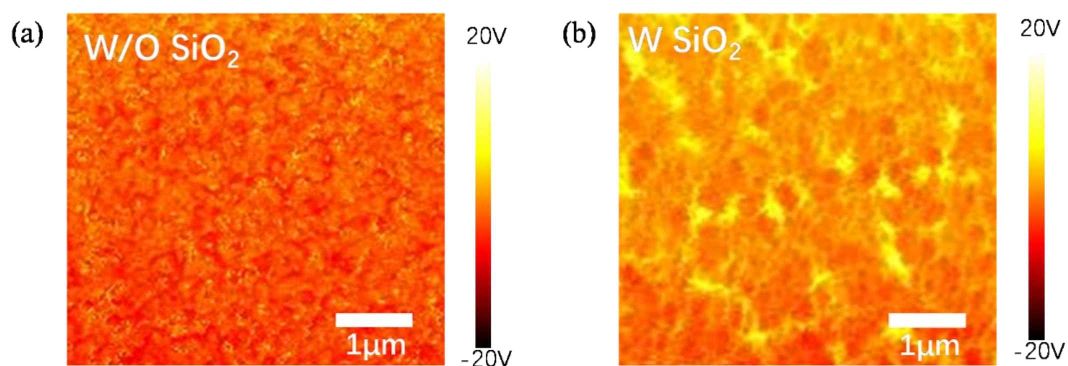

Figure S10. Scattering-type scanning near-field optical microscopy (s-SNOM) of (a) pristine 4PADCB and (b) SiO_2-modified film deposited on ITO at the wave number of 1012 cm^{-1}.

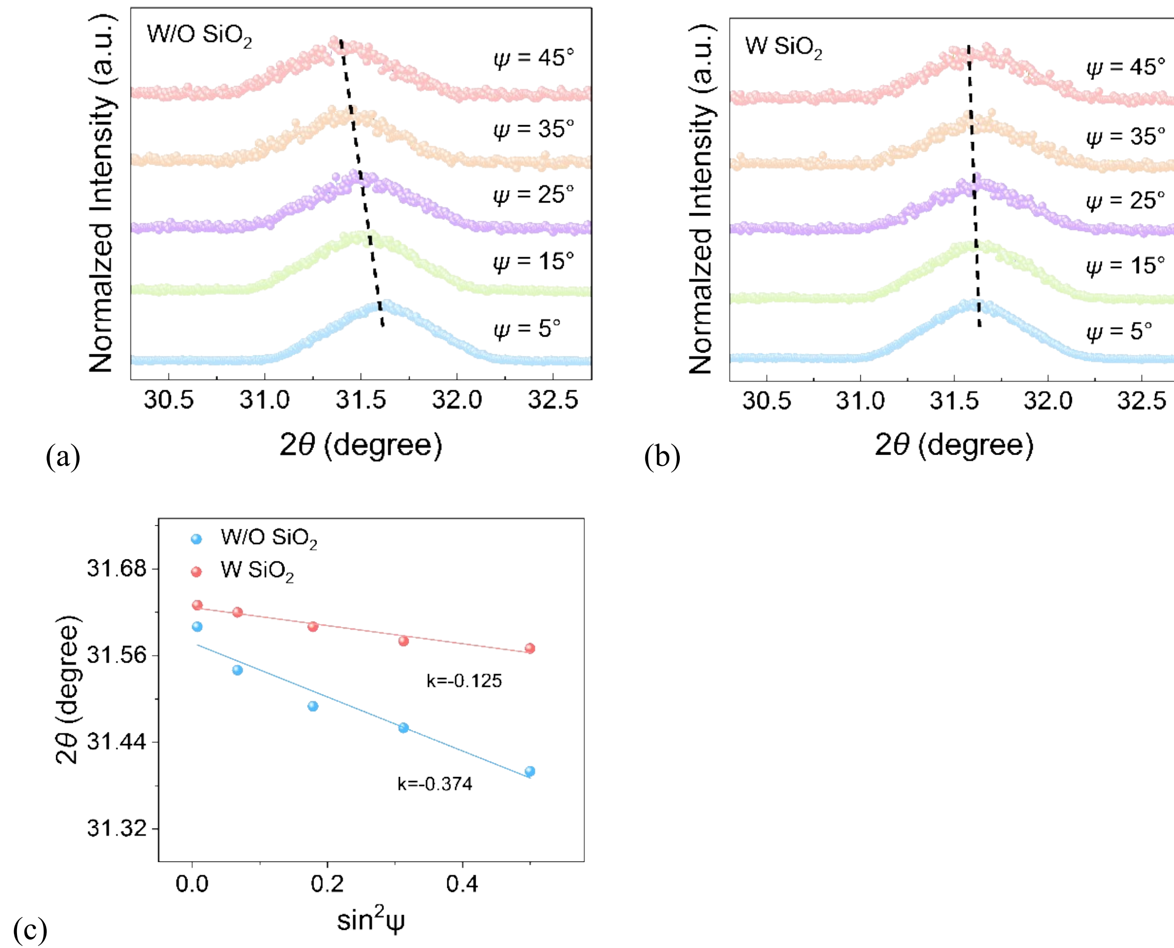

Figure S11. Depth-profiling X-ray diffraction (XRD) characterization measured at different ψ angles from 5º to 45º for perovskite films deposited on (a) pristine SAM substrate, (b) SiO_2-modified film substrate. (c) The corresponding residual strain evaluation plotted as a function of 2θ-$\sin^2\psi$.

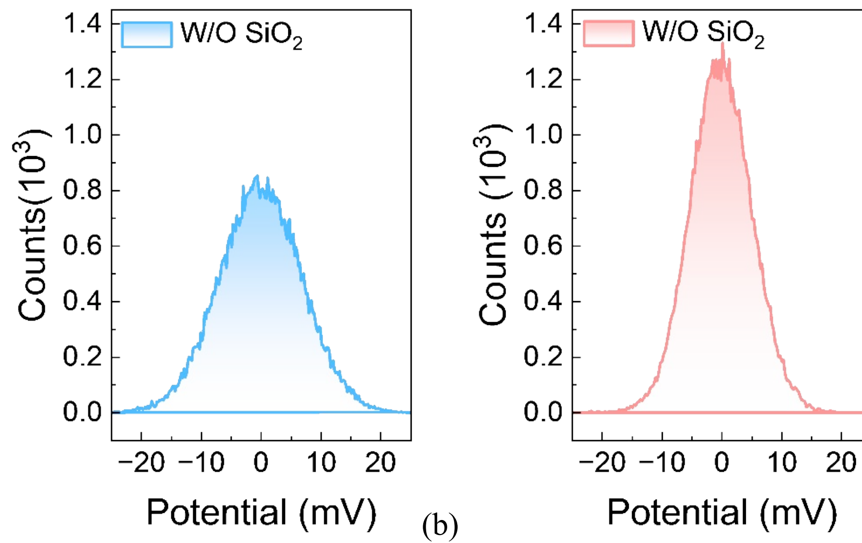

Figure S12. The potential distribution curve of (a) pristine 4PADCB and (b) SiO_2-based HTLs deposited on ITO.

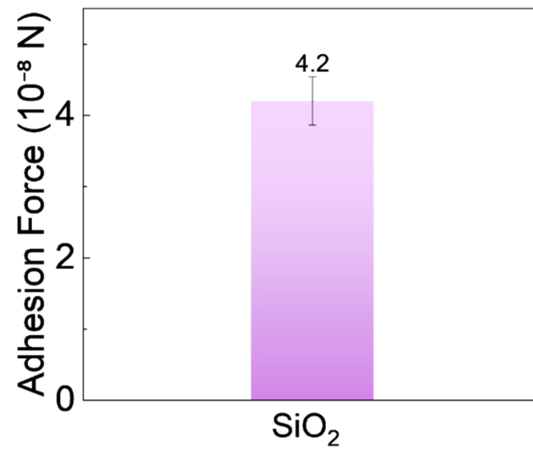

Figure S13. The adhesion force of SiO_2 layer.

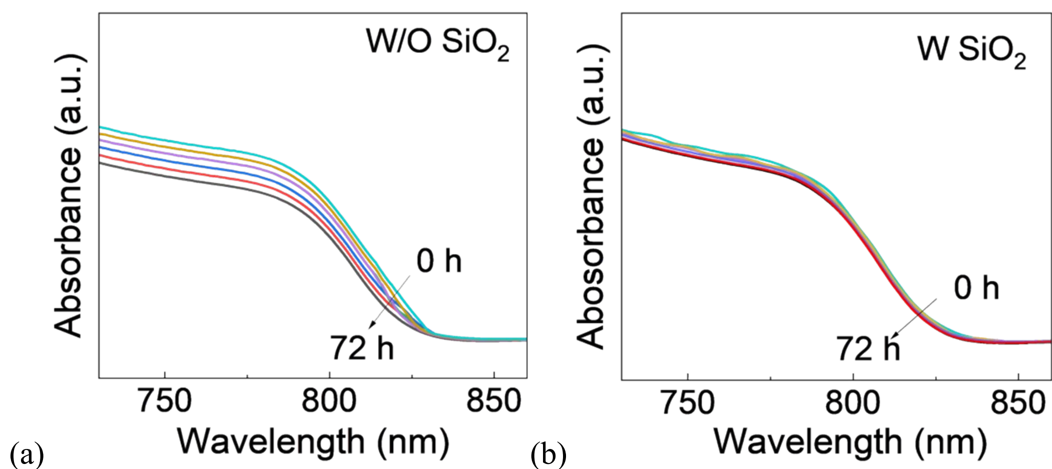

Figure S14. The UV absorption spectrum of perovskite films deposited on (a) pristine 4PADCB and (b) SiO_2-modified HTLs exposed to 20 mW/m^2 ultraviolet light-induced before and after aging in ambient air.

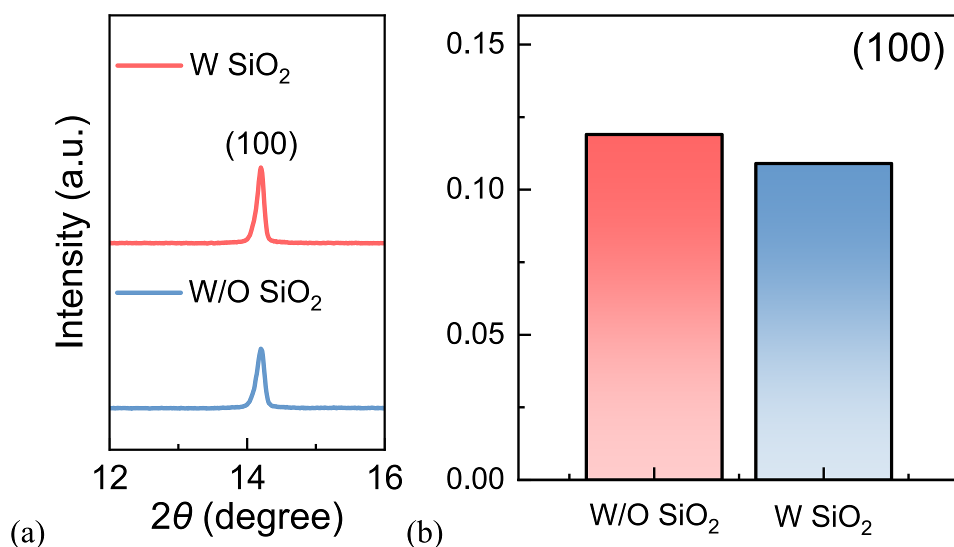

Figure S15. (a) The XRD patterns of perovskite films deposited on pristine 4PADCB and SiO_2-modified HTLs of the (100) peak. (b) Comparison of (100) peak FWHM values between control and SiO_2-modified films.

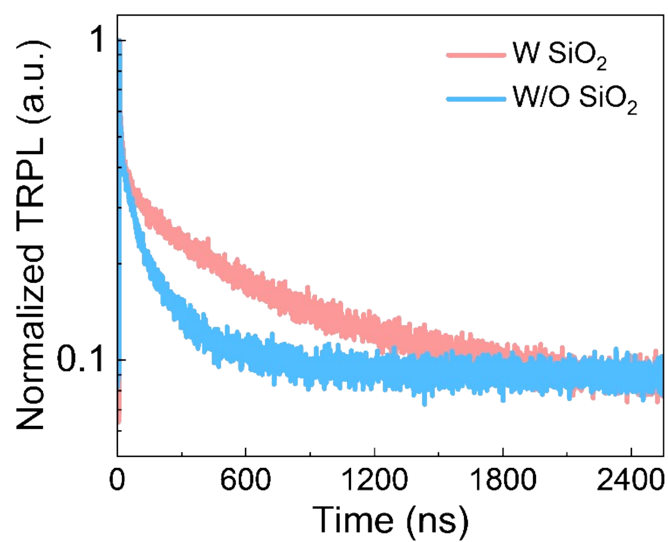

Figure S16. Time-resolved photoluminescence (TRPL) decay curves of perovskite films deposited on W/O and W SiO_2-modified HTLs.

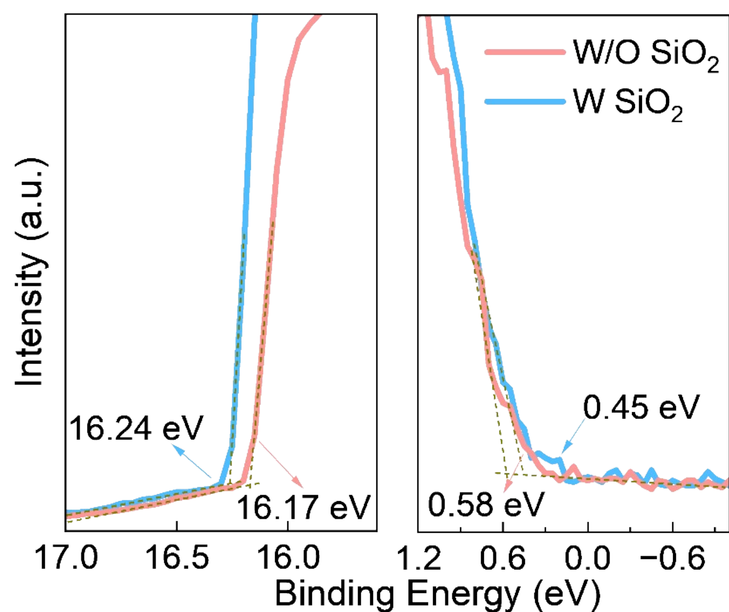

Figure S17. The ultraviolet photoelectron spectroscopy (UPS) of the samples without and with SiO_2-modified films deposited on the ITO.

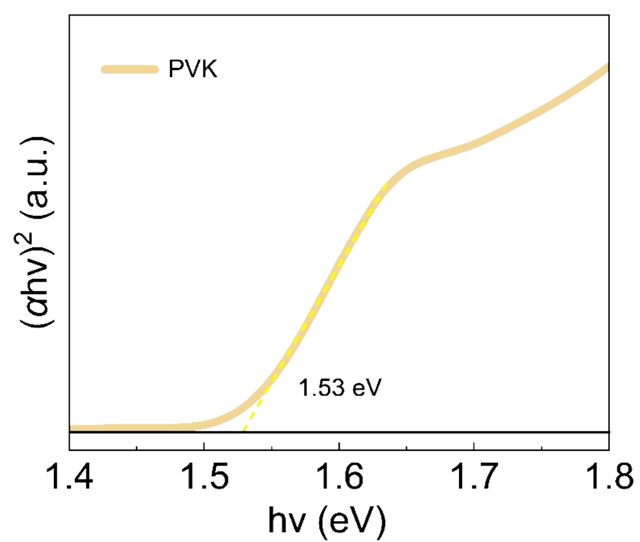

Figure S18. Tauc plots of perovskite films.

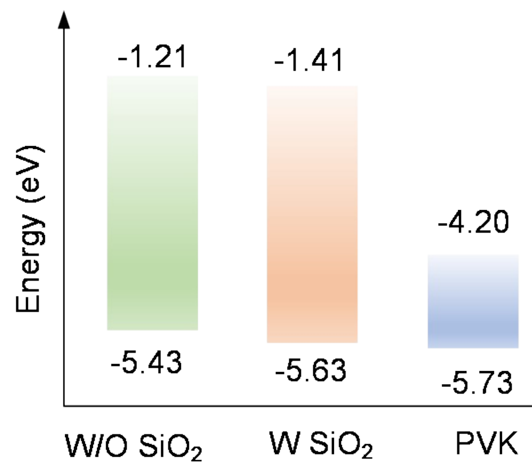

Figure S19. Energetic diagram of HTLs film and perovskite film.

福建省计量科学研究院
FUJIAN METROLOGY INSTITUTE
（国家光伏产业计量测试中心）
National PV Industry Measurement and Testing Center

25Q3-00268

检测结果/说明：
Results of Test and additional explanation.

1. 标准测试条件 Standard Test Condition (STC)：
总辐照度 Total Irradiance：1000 W/m^2
被测电池温度 Temperature：25.0 °C
光谱分布 Spectral Distribution：AM1.5G

2.STC条件下测量数据 Measurement Data and I-V/P-V Curves under STC

正扫 Forward Scan

I_{sc} (mA)	V_{oc}(V)	I_{MPP}(mA)	V_{MPP}(V)	P_{MPP} (mW)	FF(%)	A (cm^2)
2.144	1.162	2.042	1.012	2.067	82.97	0.0815

反扫 Reverse Scan

I_{sc} (mA)	V_{oc}(V)	I_{MPP}(mA)	V_{MPP}(V)	P_{MPP} (mW)	FF(%)	A (cm^2)
2.152	1.179	2.088	1.056	2.205	86.91	0.0815

失配因子 Mismatch factor: 1.009

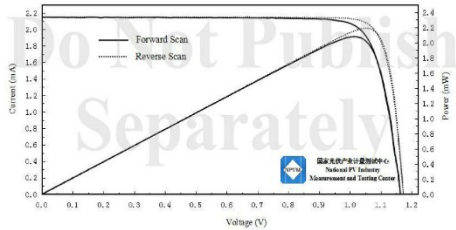

图1 STC下电流-电压特性曲线和功率-电压特性曲线
Figure 1. I-V and P-V characteristic curves of the measured sample under STC

检测报告续页专用
Continued page of test report

第 3 页/共 7 页
Page of Pages

福建省计量科学研究院
FUJIAN METROLOGY INSTITUTE
（国家光伏产业计量测试中心）
National PV Industry Measurement and Testing Center

报告编号：25Q3-00268
Report No.

检测结果/说明：
Results of Test and additional explanation.

3.STC条件下最大功率稳态输出的测量数据及曲线Measurement Data and Curves for MPPT under STC

η (%)	26.92
P_{MPP} (mW)	2.194
I_{MPP} (mA)	2.088
V_{MPP} (V)	1.051

说明：上表为300秒测试过程中最后 30 秒内 STC 条件下的最大功率稳态输出平均测试数据
Note: Measurement data for MPPT under STC in the above table was the mean value acquired during the final 30 seconds of the 300 seconds test

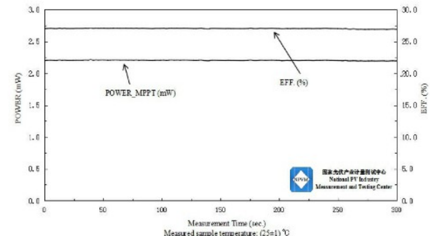

图2 被测样品最大功率稳态输出的功率-效率曲线
Figure 2. Measurement curves of the measured sample for MPPT

检测报告续页专用

第 4 页/共 7 页
Page of Pages

Figure S20. Certification of champion device performance: 26.92% steady-state PCE (0.0815 cm^2 mask area; NPVM).

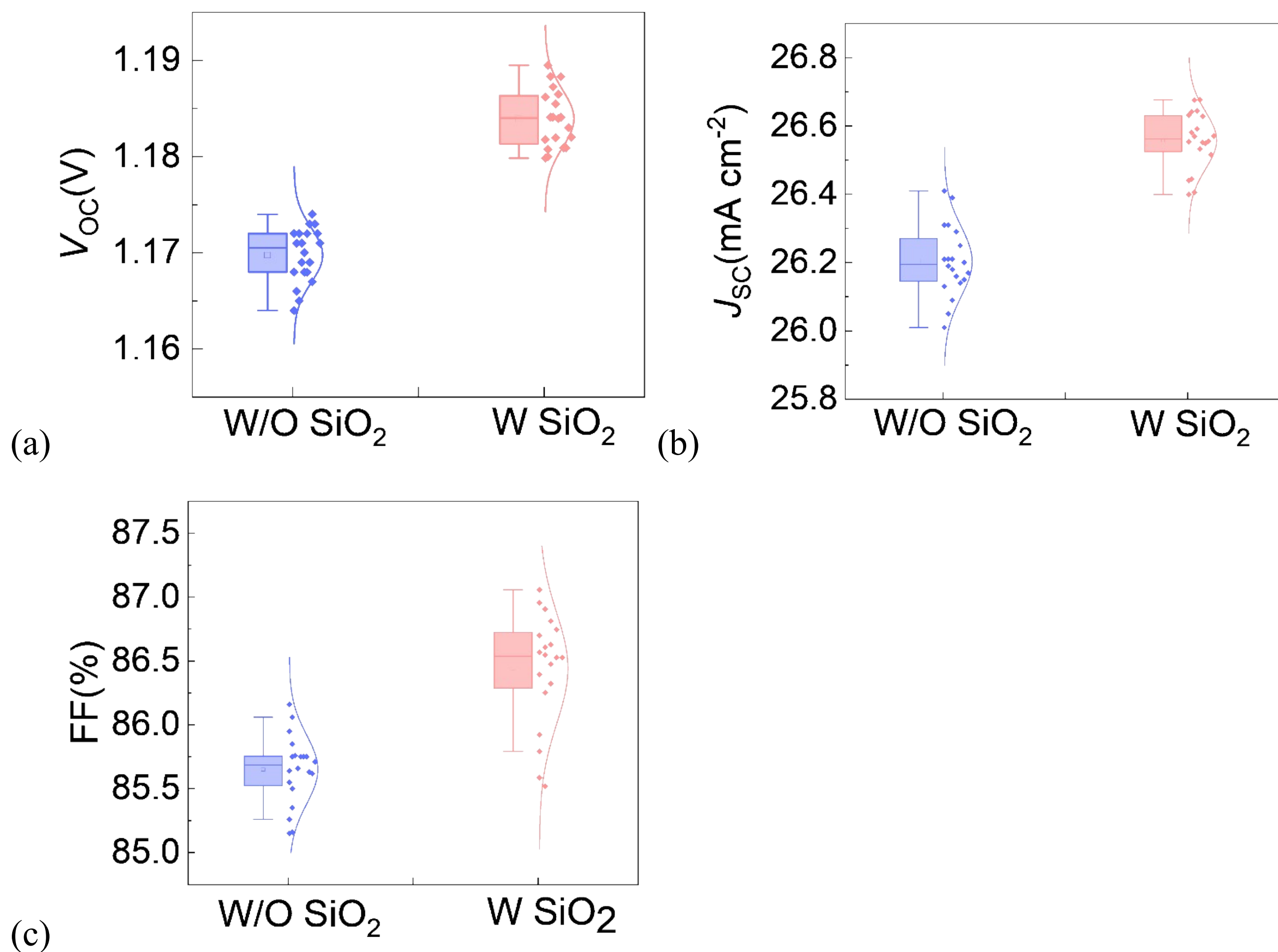

Figure S21. Distribution of the four parameters (a) V_{OC}, (b) $J_{SC,}$ and (c) FF of SAM without and with SiO_2 modified HTLs-based PSCs. The statistical data were obtained from 20 individual cells for each kind of PSCs.

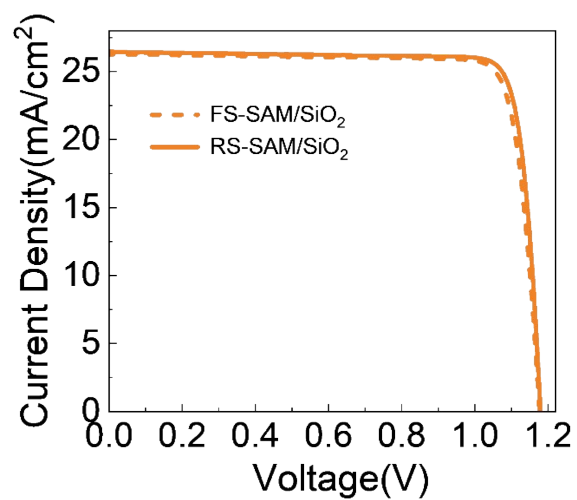

Figure S22. The forward and reverse scans curves of SAM/SiO_2 champion device under AM 1.5G illumination (100 mW/cm²).

Table S1. Fitting results of perovskite films, TRPL curves of the SAM without and with SiO_2 modified HTLs deposited on ITO grass substrate.

Sample	A_1	τ_1 (ns)	A_2	τ_2 (ns)	τ_{ave} (ns)
W SiO_2	0.149	32.61	0.240	580.01	370.34
W/O SiO_2	0.236	62.92	0.145	248.44	133.52

Table S2 Forward scanning (FS) and reverse scanning (RS) photovoltaic parameters of without and with SiO_2 modified HTLs-based champion PSCs.

Sample	V_{OC} (V)	J_{SC} (mA cm^{-2})	FF (%)	PCE (%)
RS-W/O SiO_2	1.172	26.19	85.86	26.37
FS-W/O SiO_2	1.171	26.19	85.25	26.15
RS-W SiO_2	1.187	26.57	86.77	27.37
FS-W SiO_2	1.183	26.19	85.19	26.91

Table S3. Photovoltaic parameter distributions of PSCs based on three types of HTLs: pristine 4PADCB (W/O SiO_2), pre-mixed SiO_2/SAM (W SiO_2), and sequentially deposited SAM/SiO_2.

Devices		V_{OC} (V)	J_{SC} (mA cm^{-2})	FF (%)	PCE (%)
W/O SiO_2	Average	1.170±0.003	26.20±0.103	85.65±0.230	26.22±0.119
	Champion	1.172	26.19	85.85	26.37
W SiO_2	Average	1.184±0.003	26.56±0.084	86.44±0.434	27.24±0.115
	Champion	1.187	26.57	86.77	27.35
SAM/SiO_2	Average	1.174±0.004	26.53±0.131	85.65±0.312	26.68±0.148
	Champion	1.179	26.46	86.43	26.97

References

1 F. Li, X. Deng, F. Qi, Z. Li, D. Liu, D. Shen, M. Qin, S. Wu, F. Lin and S.-H. Jang, J. Am. Chem. Soc., 2020, **142**, 20134-20142.

2 C. Luo, G. Zheng, F. Gao, X. Wang, C. Zhan, X. Gao and Q. Zhao, Nat. Photonics, 2023, **17**, 856-864.

3 L. Yang, J. Feng, Z. Liu, Y. Duan, S. Zhan, S. Yang, K. He, Y. Li, Y. Zhou and N. Yuan, Adv. Mater., 2022, **34**, 2201681.

4 Y. Luo and J. Xue, Joule, 2026, **10**, 102390.

5 S. Huang, Q. Guo, J. Ni, Z. Lin and X. Chen, Phys. Chem. Chem. Phys., 2026, **28**, 6769-6775.

6 M. Stolterfoht, P. Caprioglio, C. M. Wolff, J. A. Márquez, J. Nordmann, S. Zhang, D. Rothhardt, U. Hörmann, Y. Amir and A. Redinger, Energy Environ. Sci., 2019, **12**, 2778-2788.